Direct simulation of a Mach-5 turbulent spatially-developing boundary layer

Guillermo Araya, Christian Lagares and Kenneth Jansen *
*, † Dept. of Mechanical Eng., University of Puerto Rico at Mayagüez, PR 00681, USA
† Dept. of Aerospace Eng. Sciences, University of Colorado at Boulder, CO 80309, USA

Direct Numerical Simulation (DNS) of turbulent spatially-developing boundary layers is performed over an isothermal flat plate at several flow regimes: incompressible, supersonic (Mach 2.5), and hypersonic (Mach 5). Similar low Reynolds numbers are considered in all cases with the purpose of assessing flow compressibility on low/high order flow statistics and on the dynamics of coherent structures of Zero Pressure Gradient (ZPG) flows. Turbulent inflow information is generated by following the concept of the rescaling-recycling approach introduced by Lund et al. (J. Comp. Phys. 140, 233-258, 1998); although, the proposed methodology is extended to high-speed flows. Furthermore, a dynamic approach is employed to connect the friction velocities at the inlet and recycle stations (i.e., there is no need of an empirical correlation as in Lund et al.). The Mach number effect has been mainly identified as significant changes in peak values of the streamwise velocity fluctuations u'. The vertical transport of Reynolds shear stresses is slightly away from the wall in the near wall region for the hypersonic case. Zones of low speed fluid exhibits a much more elongated shape in incompressible flow as compared with the compressible counterpart. Furthermore, low speed streaks exhibit a contorted, twisted and stretched form in incompressible flow while they are shorter and more isotropic in the supersonic flow.

Nomenclature

 C_f Skin friction coefficient

 δ Boundary layer thickness at 99% U_{∞}

 U_{∞} Freestream velocity

 T_{∞} Freestream temperature

 ν Kinematic viscosity

 u_{τ} Friction velocity

Subscript

inl inlet

rec recycle

I. Introduction and Background

Spatially-developing turbulent boundary layers (SDTBL) are ubiquitous and show a non-homogeneous conditions along the flow direction. Computationally speaking, this type of boundary layer poses an enormous challenge, due to the need for realistic, precise, and time-dependent inflow turbulence information. Moreover, accounting for the effects of flow compressibility adds significant complexity to the problem. Consequently, high-speed SDTBL over compressible wall-bounded flows are of crucial importance in aerospace applications, such as unmanned high-speed vehicles, scramjets and advanced space aircraft. Thus, the acquired understanding of the physics behind high-speed boundary layers can lead to the development of more efficient control techniques for the fluid flow (e.g., wave drag reduction) and aerodynamic heating

^{*}Assistant Professor, AIAA Senior Member, araya@mailaps.org

[†]PhD student

[‡]AIAA Associate Fellow

on hypersonic vehicle design. Significant research effort has been devoted to hypersonic flight in the last decades, since it is directly connected to "rapid responsiveness, increased survivability in contested environments and efficient range coverage" from a military perspective, according to Schmisseur.¹⁷ What is more, a Mach 6-aircraft would be able to reach the US West Coast in approximately 23 minutes from the US East Coast,¹⁷ as seen in fig. 1. In 2013, the Boeing X-51A Waverider Scramjet prototype was released at 50,000 feet as part of the the fourth and final test flight in the U.S. Air Force program, reaching a Mach number of 5.1, which is enough to fly from New York to London in roughly 75 minutes.

One of the first DNS of supersonic spatially-evolving boundary layers was performed by Guarini $et~al.^{16}$ They considered an adiabatic wall, a Mach number of $M_{\infty}=2.5$ and a Reynolds number, based on momentum integral thickness and wall viscosity, of $Re_{\delta 2}=849$. For turbulence inflow generation, Guarini $et~al.^{16}$ made used of the Spalart²⁰'s coordinate transformation for incompressible ZPG flow, in which the growth of the boundary layer is so slow that the turbulence can be treated as approximately homogeneous in the streamwise direction. Urbin & Knight⁹ and Stolz & Adams²¹ proposed different modifications to the rescaling-recycling approach (introduced by Lund $et~al.^{13}$ for incompressible boundary layers) in order to account for compressibility effects on inlet conditions. Martin's research group has performed important investigations on supersonic-hypersonic flows by analyzing the effects of Mach



Figure 1. Comparison of range covered by hypersonic capabilities in US (source: Schmisseur¹⁷).

number, high enthalpy and initialization on zero-pressure gradient (ZPG) boundary layers, which were performed at low momentum-thickness Reynolds numbers ($Re_{\delta 2} \sim 1600$) or $Re_{\tau} = \delta u_{\tau}/\nu_{w} \sim 500$ in spatial domains with streamwise lengths in the order of 10δ , being δ the inlet boundary layer thickness. Priebe & Martin¹⁵ studied low-frequency unsteadiness by carrying out direct simulations over a 24° compression ramp at Mach 2.9 and $Re_{\tau} = 340$. They used the recycling-rescaling technique by Xu & Martin²⁴ and considered an auxiliary domain ($\sim 8.3\delta$ in length with the recycle plane at 7.3δ) to feed turbulent information to a principal domain ($\sim 14.3\delta$ in length) obtaining a mesh with 28 million points in total. Also, Beekman et al.² investigated the effects of the recycling length and the largest turbulent structures on the recycling technique of 24 by performing a DNS of SDTBL at Mach 2.9 and $Re_{\tau} \sim 640$ on a large computational domain (about 60-inlet boundary layer thicknesses in streamwise length). Based on Simens et al. 19 large eddy evolution time scale definition of δ/u_{τ} , Beekman et al.² estimated that a necessary rescaling length should be in the order of $O(12\delta)$ to permit the natural evolution of a large scale motion before recycling it. They also showed that the recycle plane was nearly disjoint from the most energetic turbulent scales when located at 57δ . Certainly, the principal challenge in unsteady numerical predictions of compressible turbulent spatiallydeveloping boundary layers is the prescription of accurate time-dependent inflow conditions (instantaneous profiles of velocity, temperature and pressure). In this study, we are proposing a dynamic approach to connect the friction velocities at the inlet and recycle stations, which permits to account for the effects of arbitrary Reynolds and Mach numbers. Therefore, there is no need of an empirical correlation as in Lund etal., 13 Urbin & Knight and Stolz & Adams. 21 The major objective of the present manuscript is to evaluate the transport phenomena (momentum and thermal) inside turbulent boundary layers at three clearly distinctive flow regimes: incompressible, supersonic and hypersonic. Moreover, flow visualization is also carried out to assess the effects of compressibility in coherent structures.

II. Mesh Generation, Flow Solver, Inflow Generation and Boundary Conditions

Capturing the physics of turbulent spatially-developing boundary layers by using DNS is not a trivial task, due to the following reasons: i) high mesh resolution required in order to resolve the smallest turbulence scales (Kolmogorov scales), ii) the computational box must be large enough to appropriately resolve the influence of the turbulent "superstructures" (Hutchins & Marusic¹⁰) located in the outer region of the boundary layer, iii) realistic time-dependent inflow turbulent conditions (instantaneous velocity, temperature and pressure) must be prescribed. Figure 2 shows the schematic of the computational domain in order to simulate spatially-developing boundary layers in the incompressible, supersonic and hypersonic regime.

Flow Solver: To successfully perform the proposed DNS, a highly accurate, very efficient, and highly scalable CFD solver is required. PHASTA is an open-source, parallel, hierarchic $(2^{nd} \text{ to } 5^{th} \text{ order accurate})$, adaptive, stabilized (finite-element) transient analysis tool for the solution of compressible²³ or incompressible flows (Jansen¹¹).

Inflow Generation: As articulated previously, one of the crucial aspects on the simulations of unsteady spatially-developing turbulent boundary layers is the prescription of accurate and realistic turbulent inflow information. In this study, we will make use of the inflow generation method devised by Araya $et\ al.$, which is a modified version of the original rescaling-recycling method by Lund $et\ al.$ The seminal idea of the rescaling-recycling method is to extract the flow solution (mean and fluctuating components of the velocity, thermal and pressure fields) from a downstream plane (called "recycle") and after performing a transformation by means of scaling functions, the transformed profiles are re-injected at the inlet plane, as seen in figure 2. The objective of implementing scaling laws to the flow solution is to convert the streamwise in-homogeneity of the flow into quasi-homogeneous conditions. The domain length was prescribed long enough (about $45\delta_{inlet}$) in order to appropriately capture the influence of large scale motions (LSM) or superstructures.

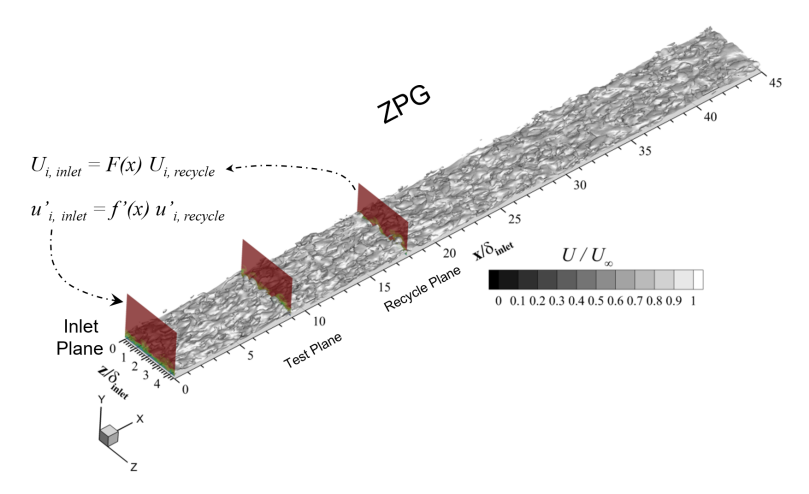


Figure 2. Schematic of the spatially-developing boundary layer with Inlet, Recycle and Test planes about $45\delta_{inlet}$ of streamwise length.

Boundary Conditions: At the wall, the classical no-slip condition is imposed for velocity components. Isothermal wall is assumed for the thermal field. For both compressible flow cases, the ratio T_w/T_∞ is 2.25, where T_w is the wall temperature and T_∞ is the freestream temperature. The T_r/T_∞ ratios are 2.12 and 5.45 for M_∞ equals to 2.5 and 5, respectively. T_r is the recovery or adiabatic temperature. The lateral boundary conditions are handled via periodicity.

Table 1 summarizes the characteristics of the proposed three (3) cases: the incompressible case ($M_{\infty}=0$) and compressible cases ($M_{\infty}=2.5$ and 5). Information regarding the Reynolds number range, computational domain dimensions in terms of the inlet boundary layer thickness δ_{inl} (where L_x , L_y and L_z represent the streamwise, wall-normal and spanwise domain length, respectively) and mesh resolution in wall units (Δx^+ , Δy^+_{min} , Δy^+_{max} , Δz^+) is also supplied. In all cases, the number of mesh points in the streamwise, wall-normal and spanwise direction is $440 \times 60 \times 80$, respectively. The three cases were run in 96 processors in Stampede 2 (TACC), consuming about 20,000 CPU hours each.

Case	M_{∞}	$Re_{\delta 2}$	$L_x \times L_y \times L_z$	$\Delta x^+, \Delta y_{min}^+/\Delta y_{max}^+, \Delta z^+$
1	0	306-578	$45\delta_{inl} \times 3.5\delta_{inl} \times 4.3\delta_{inl}$	14.7, 0.2/13, 8
2	2.5	434-816	$42\delta_{inl} \times 3.5\delta_{inl} \times 4.3\delta_{inl}$	15, 0.2/14, 9
3	5	344-616	$44\delta_{int} \times 3.5\delta_{int} \times 4.3\delta_{int}$	13.3, 0.17/16.7, 7.4

Table 1. Numerical Cases.

III. Results and Discussion

During the re-scaling process of the flow parameters in the inflow generation methodology, ¹ the ratio of the inlet friction velocity to the recycle friction velocity (i.e., $\lambda = u_{\tau,inl}/u_{\tau,rec}$) is required. Here, the friction velocity is defined as $u_{\tau} = \sqrt{\tau_w/\rho}$, where τ_w is the wall shear stress and ρ is the fluid density. Since the inlet boundary layer thickness must be prescribed according to the desired inlet Reynolds number, prescribing also the inlet friction velocity would be redundant. In order to overcome this issue, Lund *et al.*, ¹³ Urbin & Knight⁹ and Stolz & Adams²¹ used the well-known 1/8-power law that connects the friction velocity to the momentum thickness in zero-pressure gradient flows, thus $u_{\tau,inl}/u_{\tau,rec} = (\delta_{2,inl}/\delta_{2,rec})^{-1/8}$. Since the power (-1/8) could be affected by the Reynolds number dependency or compressibility effects, we are proposing the explicit computation of this power, $\gamma_{\delta 2}$, by relating the mean flow solution from a new plane (so-called the "Test" plane, as seen in figure 2) to the solution from the recycle plane as follows:

$$\gamma_{\delta 2} = \frac{\ln(u_{\tau,test}/u_{\tau,rec})}{\ln(\delta_{2,test}/\delta_{2,rec})}.$$
 (1)

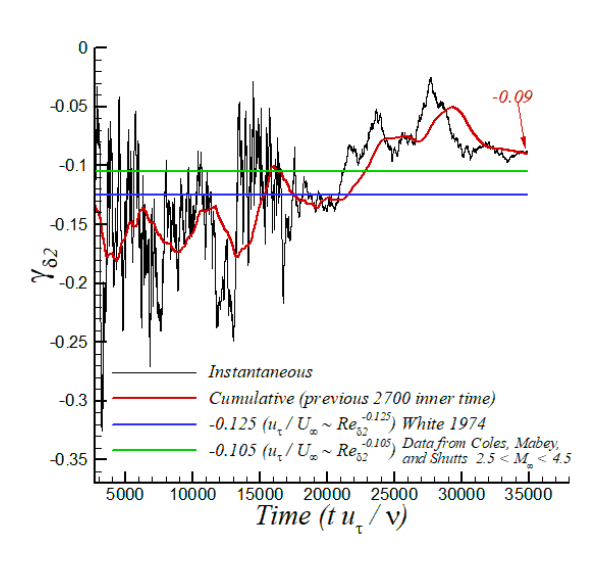


Figure 3. Time-series of the dynamically computed power-law exponent $\gamma_{\delta 2}$ for supersonic Case 2.

Figure 3 shows a representative time series of the dynamically computed power law exponent $\gamma_{\delta 2}$ computed by Eq. 1 in Case 2 for the supersonic flat plate. It is observed that $\gamma_{\delta 2}$ fluctuates wildly during the transient stage, and, later tends to the approximate value of -0.09 (by averaging the previous 2700 inner time), which differs in about 32% from the classical empirical value of -1/8 (see White²²). However, this cumulative value of $\gamma_{\delta 2}$ is very close to the empirical value (-0.105) obtained from experiments by Coles, Mabey and Shutts^{3,7,8} at a Mach number range of $2.5 < M_{\infty} < 4.5$ but at significantly higher Reynolds numbers. For the incompressible case, a value of -0.083 was computed for $\gamma_{\delta 2}$ whereas a value of -0.063 was obtained in the hypersonic boundary layer (not shown here). Interestingly, this may reveal a moderate compressibility effect on the power $\gamma_{\delta 2}$, particularly for high-speed flows. Once the exponent $\gamma_{\delta 2}$ is obtained from Eq. 1, the values of $u_{\tau,inl}$ and λ can be calculated.

In figure 4 (a), the skin friction coefficient $C_f = (2(u_\tau/U_\infty)^2(\rho_w/\rho_\infty))$ is shown for validation purposes. A short and negligible developing section of about $2\delta_{inlet}$ in length (defined as that inlet region where the turbulent structures behave in a non-physical sense) can be observed for the C_f parameter in the supersonic flat plate at $M_\infty = 2.5$. Downstream, the skin friction coefficient exhibits the typical monotonic decay of ZPG flows with some "upticks" at the end of the computational domain induced by the singularity of the outflow plane. It can be seen a very good agreement with DNS data from Guarini et al.¹⁶ at a similar Reynolds number. Furthermore, the mean streamwise velocity in wall units is shown in figure 4 (b), where the Van Driest transformation is employed for the supersonic flow data. Our DNS data of Case 2 compares very well with other DNS from Guarini et al.¹⁶ and Duan et al.⁵

Figure 5 (a) depicts mean temperature versus mean streamwise velocity profiles at $M_{\infty} = 2.5$. Present DNS shows a good agreement with the Walz's equation as well as with experimental data at similar supersonic

Mach numbers (12 and 18). The turbulence intensities in inner-outer units are shown in fig. 5 (b). Moreover, the profiles of v'^+_{rms} and w'^+_{rms} depict a fairly good agreement with DNS data from Guarini *et al.*¹⁶ and Duan *et al.*⁵ While our peak value of u'^+_{rms} is very similar to that predicted in 16 and 5 (i.e., $u'^+_{rms,max} \approx 2.7$), some discrepancies were found in the wall-normal location. We computed the maximum u'^+_{rms} at 4.5% of δ , whereas 16 and 5 predicted a closer location to the wall (i.e., at 2.6% of δ).

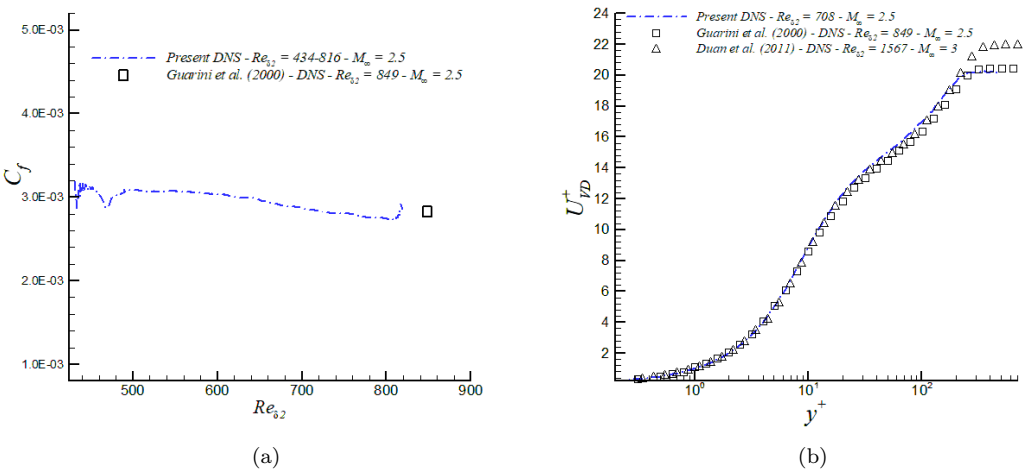


Figure 4. (a) Streamwise variation of C_f ; and, (b) mean streamwise velocity in wall units.

Figure 6 (a) exhibits the mean static temperature at $M_{\infty}=5$. It is interesting to highlight the existence of a near wall local thermal peak at $y/\delta \approx 0.04$. This is consistent with heat being removed from the fluid via the wall since our wall temperature is lower than the recovery or adiabatic temperature at this Mach number. The Walz equation for this combination of wall temperature-Mach number gives a poor prediction. Furthermore, Duan *et al.*⁴ obtained a similar thermal trend at a slightly lower wall temperature than in our DNS, as can be seen in fig. 6 (b).

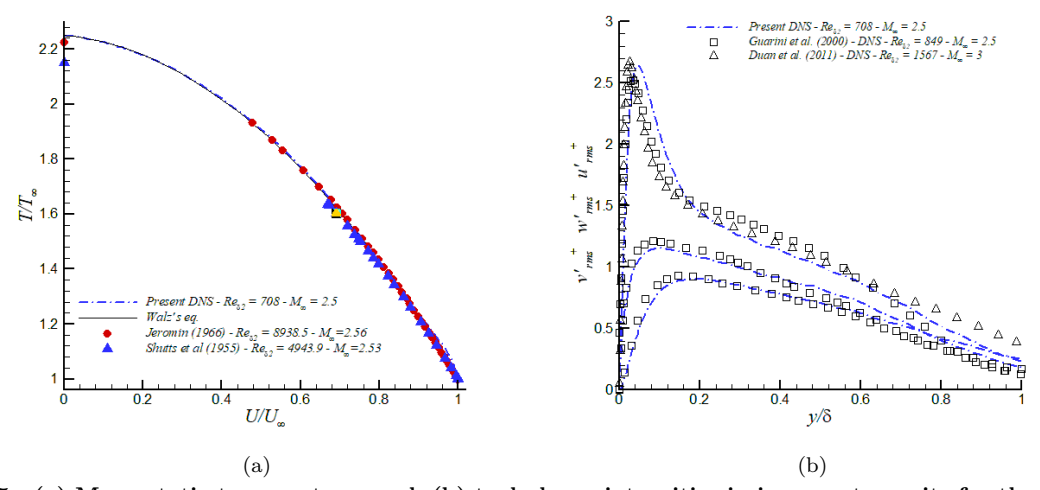


Figure 5. (a) Mean static temperature; and, (b) turbulence intensities in inner-outer units for the supersonic case.

The compressibility effects are examined in typical inner and outer boundary layer parameters. Figure 7 (a) depicts the streamwise variation of C_f for the different cases of Table 1. There is a significant decrease in the skin friction coefficient for the compressible cases 2 and 3 with respect to the incompressible case. Notice the density correction in the C_f formula (i.e., $\rho_w/\rho_\infty = T_\infty/T_w = 0.44$). The momentum thickness Reynolds number $Re_{\delta 2}$ is shown in fig. 7 (b). Compressible cases at Mach numbers 2.5 and 5 exhibit an evident developing section of approximately 5- δ_{inlet} in length (more pronounced in the hypersonic boundary

layer). Downstream, all cases show nearly linear increases of $Re_{\delta 2}$, with the supersonic case having the steeper slope.

The turbulence intensities in fig. 8 (a) reveal that peak values of streamwise velocity fluctuations u' experience significant changes (not only their intensities but also in their y/δ -locations) at the different flow regimes. For instance, peaks of u' move further from the wall in the hypersonic case ($\approx 0.01\delta$) with respect to u' peaks of the incompressible regime. The opposite is observed in the supersonic case. On the other hand, w' profiles exhibit larger intensities in the supersonic case for $y/\delta < 0.2$, as compared with incompressible and hypersonic boundary layers. The Reynolds shear stresses in the incompressible regime depict an obvious "plateau" or constant shear layer around $y/\delta \approx 0.2$, while this phenomenon is not quite evident in the compressible cases, as seen in fig. 8 (b).

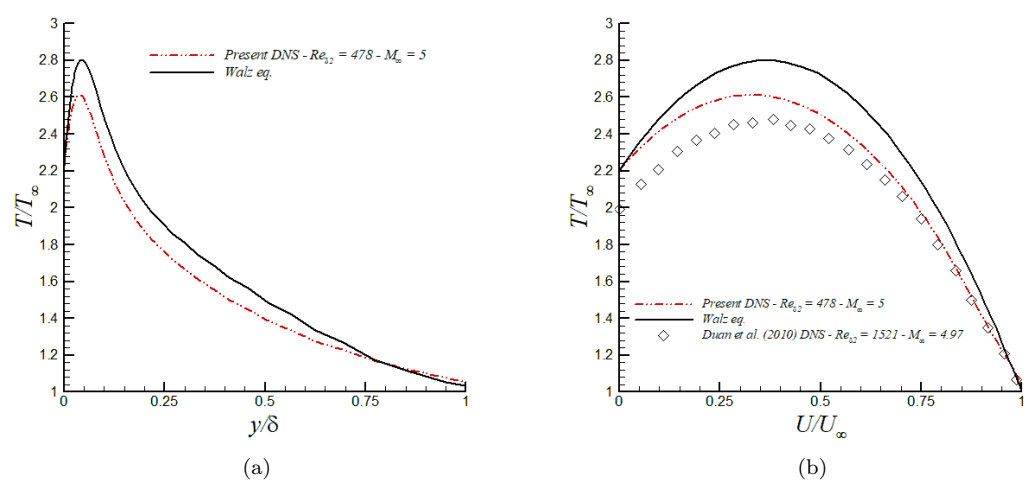


Figure 6. (a) Mean static temperature vs. y/δ ; and, (b) mean static temperature vs. U/U_{∞} for the hypersonic case.

Root Mean Square (RMS) profiles of pressure fluctuations are shown in figure 9 (a) for the compressible cases. A fairly good agreement was achieved with DNS data from Guarini $et\ al.^{16}$ at adiabatic wall conditions. The hypersonic case exhibits a significant decrease of the pressure fluctuation in the near wall region, where a local peak of the mean temperature exists. The turbulent Mach number increases as the Mach number increases by considering the same wall thermal conditions, as seen in fig. 9 (b).

Figure 10 (a) show triple correlations of velocity fluctuations in outer units. The observed level of smoothness in profiles demonstrates that the collected sample for statistical computation is quite appropriate. The vertical transport of Reynolds normal stresses, i.e. $< v'u'^2 > /U_{\infty}^2$, is mainly towards the wall in the near wall region in all cases. This vertical transport switches direction around $y/\delta \approx 0.06-0.08$ in the different flow regimes. The maximum value of $< v'u'^2 >$ is seen in the supersonic case at $y/\delta \approx 0.04$. The vertical transport of the Reynolds shear stresses < v'u'v' > are depicted by fig. 10 (b). The most relevant feature is related to the opposite direction in the vertical transport of < u'v' > in the hypersonic boundary layer (away from the wall). Further investigation will be performed to elucidate the root cause of this behavior, which could be related to the local temperature increases observed in fig. 6 (a).

A two-point correlation (TPC) analysis was performed in velocity fluctuations. Figure 11 exhibits TPC profiles of velocity fluctuations along the spanwise direction at a streamwise location of $x/\delta_{inlet} \approx 30$ and $y^+ = 15$. Fluctuations are mostly decorrelated around $z^+ = 50$, which indicates the suitability of the domain width $(L_z^+ \approx 700)$. Additionally, the spanwise spacing of low speed streaks is very similar in all cases $(\lambda^+ \approx 100)$. Perhaps, the hypersonic regime shows a larger separation of streaks. The iso-contours of R_{uu} show similar trends in all flow regimes for the plane YZ in fig. 12.

Flow visualization gives important insights of the turbulent structures in boundary layers. Visualization of near wall turbulent structures or turbulent streaks is performed by extracting iso-surfaces of instantaneous streamwise velocity fluctuations ($u' = \pm 0.2 U_{\infty}$) for Cases 1 and 2. Low speed streaks exhibit a contorted, twisted and stretched form in incompressible flow ($M_{\infty} = 0$) while they are shorter and more isotropic in the supersonic flow ($M_{\infty} = 2.5$). Several streak breakup events are identified in the close-up images.

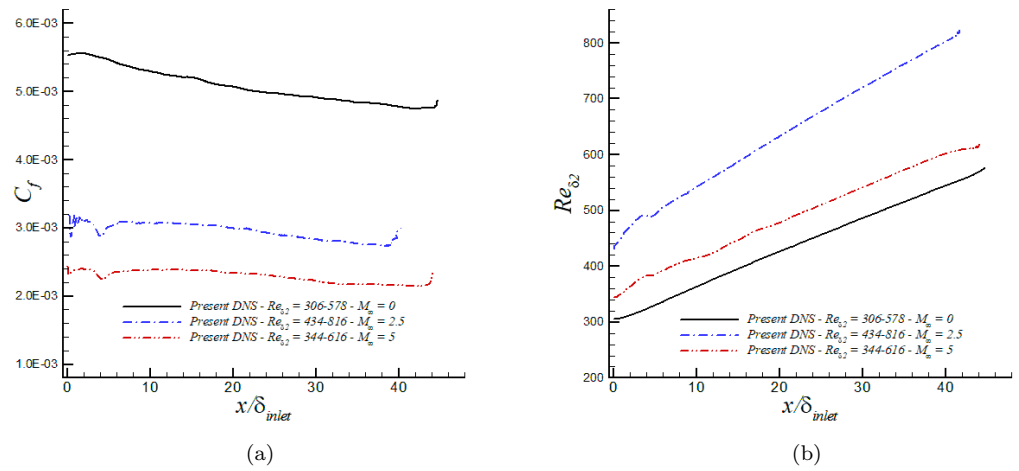


Figure 7. Effect of Mach numbers on (a) C_f , and (b) momentum thickness Reynolds number $Re_{\delta 2}$.

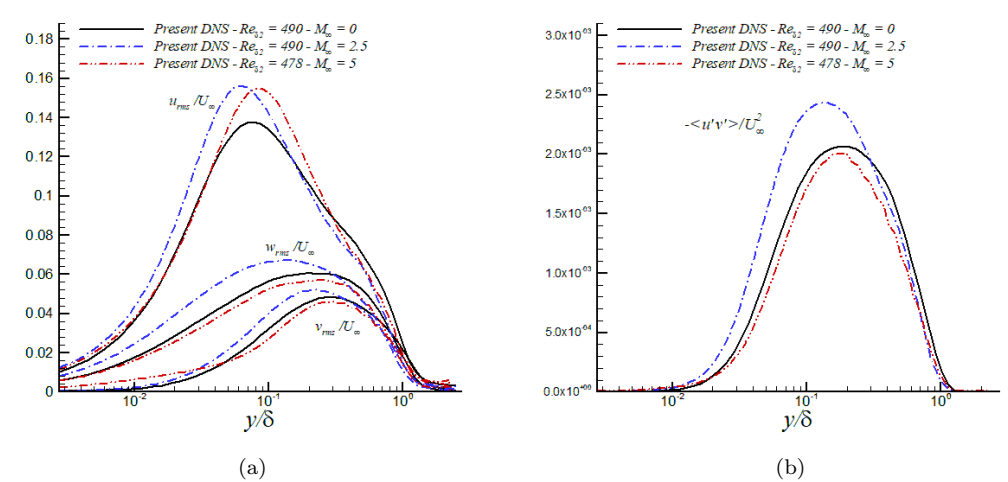


Figure 8. Effect of Mach numbers on (a) turbulence intensities, and (b) Reynolds shear stresses.

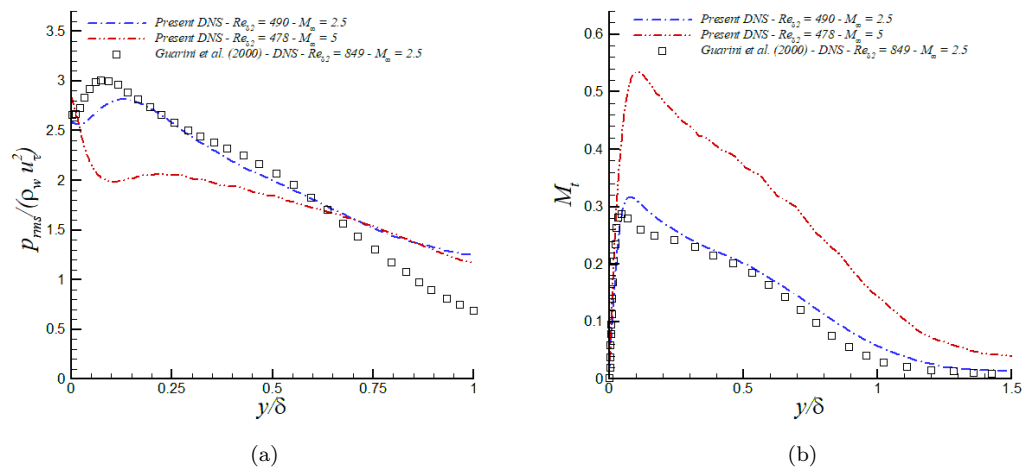


Figure 9. Effect of Mach numbers on (a) pressure fluctuations, and (b) turbulent Mach number.

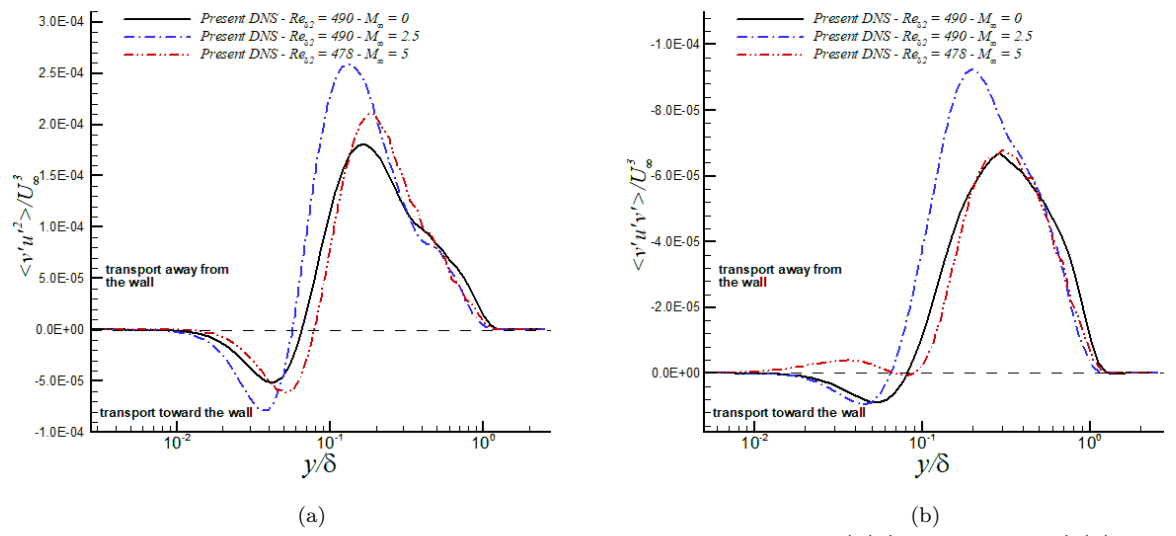


Figure 10. Effect of Mach numbers on triple correlations (a) < v'u'u' >, and (b) < v'u'v' >.

IV. Conclusions

DNS of incompressible and compressible ZPG spatially-developing turbulent boundary layers (supersonic and hypersonic regimes) has been carried out at similar Reynolds numbers. The DNS validation with experimental data and other DNS for the supersonic/hypersonic cases has been highly encouraging, particularly for validation of the proposed turbulent inflow generation. The Mach number effect has been mainly manifested in peak values of the streamwise velocity fluctuations u'. The vertical transport of Reynolds shear stresses has been observed to be away from the wall in the near wall region in the hypersonic boundary layer. Zones of low speed fluid exhibits a much more elongated shape in incompressible flow as compared with the compressible counterpart. Furthermore, low speed streaks exhibit a contorted, twisted and stretched form in incompressible flow while they are shorter and more isotropic in the supersonic flow. Future work in this study will involve the analysis of energy budget of velocity and thermal fluctuations for the incompressible, supersonic and hypersonic regime, respectively.

V. Acknowledgment

This material is based upon work supported by the Air Force Office of Scientific Research under award number FA9550-17-1-0051. Computational resources are supplied by XSEDE project #TG-CTS170006 and a Broadening Participation Allocation at Blue Waters.

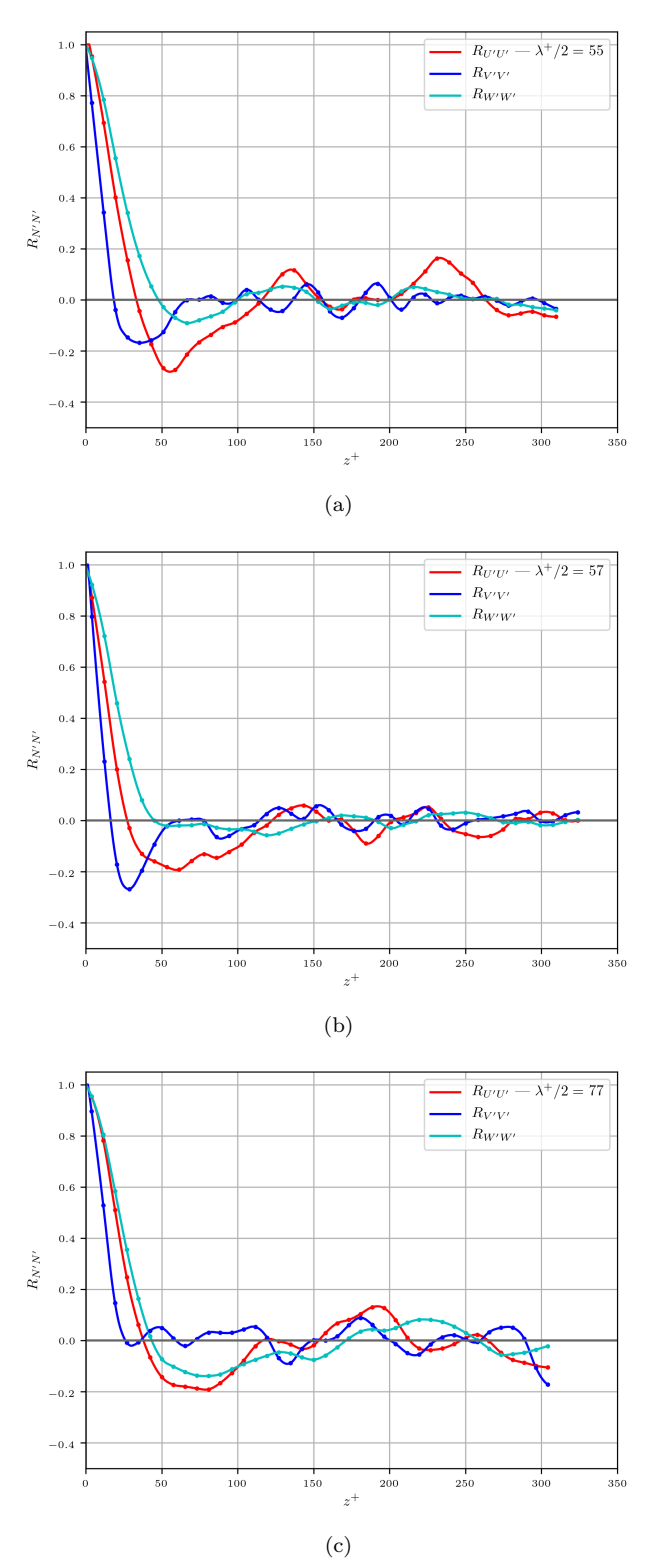


Figure 11. Two-point correlations of velocity fluctuations along the spanwise direction at $x/\delta_{inlet}\approx$ 30 and $y^+=15$: (a) $M_{\infty}=$ 0, (b) $M_{\infty}=$ 2.5 and (c) $M_{\infty}=$ 5.

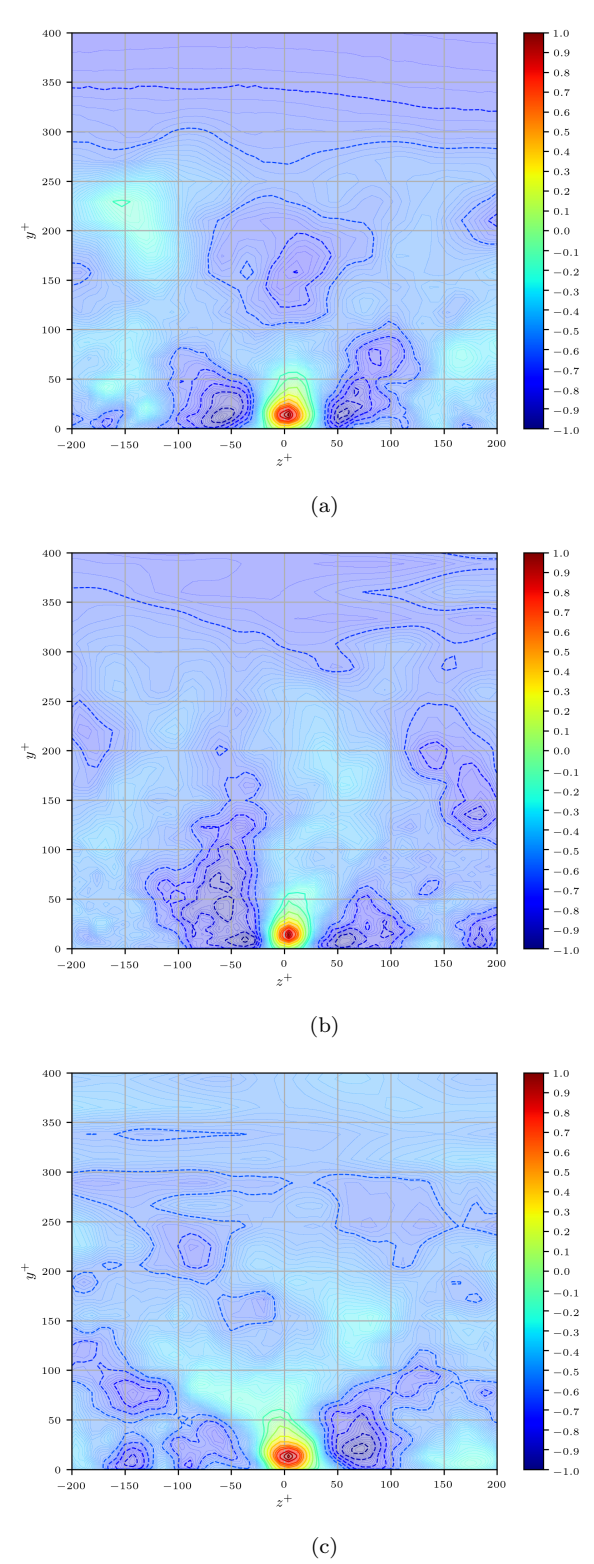


Figure 12. Two-point correlations of streamwise velocity fluctuations u' in the plane YZ at $x/\delta_{inlet}\approx$ 30: (a) $M_{\infty}=$ 0, (b) $M_{\infty}=$ 2.5 and (c) $M_{\infty}=$ 5.

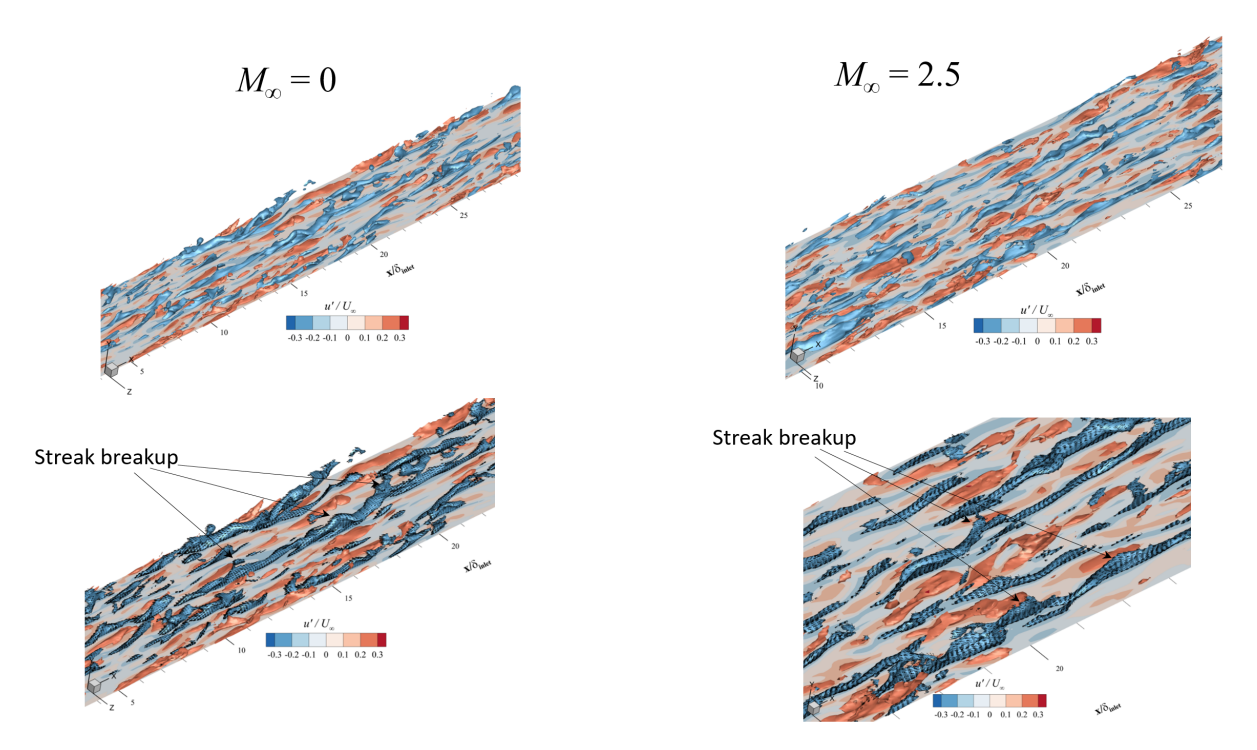


Figure 13. Visualization of near wall turbulent structures: iso-surfaces of instantaneous streamwise velocity fluctuations, $u'=\pm 0.2 U_{\infty}$.

References

- ¹G. Araya, L. Castillo, C. Meneveau, and K. Jansen. A dynamic multi-scale approach for turbulent inflow boundary conditions in spatially evolving flows. *Journal of Fluid Mechanics*, 670:518–605, 2011.
- ²I. Beekman, S. Priebe, Y.C. Kan, and M. P. Martin. Dns of a large-domain, mach 3 turbulent boundary layer: turbulence structure. In 49th AIAA Aerospace Sciences Meeting, pages 2011–753. AIAA, 2011.
 - ³D. Coles. Measurement of turbulent friction on a smooth flat plate in supersonic flow. J. Aeronaut. Sci., 7, 1954.
- ⁴Duan, L. and Beekman, I. and Martin, M. P. Direct numerical simulation of hypersonic turbulent boundary layers. part 2. effect of wall temperature. *Journal of Fluid Mechanics*, 655:419–445, 2010.
- ⁵Duan, L. and Beekman, I. and Martin, M. P. Direct numerical simulation of hypersonic turbulent boundary layers. part 3. effect of mach number. *Journal of Fluid Mechanics*, 672:245–267, 2011.
- ⁶Duan, L. and Martin, M. P. Direct numerical simulation of hypersonic turbulent boundary layers. part 4. effect of high enthalpy. *Journal of Fluid Mechanics*, 684:25–59, 2011.
- ⁷H. Fernholz and P. Finley. A critical compilation of compressible turbulent boundary layer data. *Technical Report AGARDograph, AGARD*, 223, 1977.
- ⁸H. Fernholz and P. Finley. A further compilation of compressible boundary layer data with a survey of turbulence data. *Technical Report AGARDograph, AGARD*, 263, 1981.
- ⁹G. Urbin and D. Knight. Large-Eddy Simulation of a supersonic boundary layer using an unstructured grid. AIAA Journal, 39(7):1288–1295, 2001.
- ¹⁰N. Hutchins and Ivan Marusic. Evidence of very long meandering features in the logarithmic region of turbulent boundary layers. *Journal of Fluid Mechanics*, 579:1–28, 2007.
- ¹¹K. E. Jansen. A stabilized finite element method for computing turbulence. Comp. Meth. Appl. Mech. Engng., 174:299–317, 1999.
 - ¹²Jeromin, L. Compressible turbulent boundary layer with fluid injection. PhD thesis, Cambridge University, 1966.
- ¹³T.S. Lund, X. Wu, and K.D. Squires. Generation of turbulent inflow data for spatially-developing boundary layer simulations. *Journal of Computational Physics*, 140(2):233–258, 1998.
- ¹⁴Martin, M. P. Direct numerical simulation of hypersonic turbulent boundary layers. part 1. initialization and comparison with experiments. *Journal of Fluid Mechanics*, 570:347–364, 2007.
- ¹⁵Priebe, S. and Martin, M. P. Low-frequency unsteadiness in shock wave-turbulent boundary layer interaction. *Journal of Fluid Mechanics*, 699:1–49, 2012.
- ¹⁶S. Guarini and R. Moser and K. Shariff and A. Wray. Direct numerical simulation of a supersonic turbulent boundary layer at mach 2.5. *Journal of Fluid Mechanics*, 414:1–33, 2000.
- 17 J.D. Schmisseur. Hypersonics Into the 21^{st} Century: A Perspective on AFOSR-Sponsored Research in Aerothermodynamics. In 43^{rd} AIAA Fluid Dynamics Conference June 24-27, 2013, San Diego, CA., pages AIAA 2013–2606. AIAA, 2013.
- 18 W. Shutts, W. Hartwig, and J. Weiler. Turbulent boundary layer and skin friction measurements on a smooth, thermally insulated flat plate at supersonic speeds. DRL, 364, 1955.
- ¹⁹J. Simens, M. amd Jimenez, S. Hoyas, , and Y. Mizuno. A high-resolution code for turbulent boundary layers. *J. of Comp. Physics*, 228:4218–4231, 2009.
- 20 P.R. Spalart. Direct simulation of a turbulent boundary layer up to $Re_{\theta} = 1410$. Journal of Fluid Mechanics, 187:61–98,
- ²¹S. Stolz and N. Adams. Large-eddy simulation of high-Reynolds-number supersonic boundary layers using the approximate deconvolution model and a rescaling and recycling technique. *Physics of Fluids*, 15(8):2398–2412, 2003.
 - ²²F. M. White. *Viscous Fluid Flow*. McGraw-Hill Mechanical Engineering, New York, 2006.
- ²³C. H. Whiting, K. E. Jansen, and S. Dey. Hierarchical basis in stabilized finite element methods for compressible flows. Comp. Meth. Appl. Mech. Engng., 192(47-48):5167-5185, 2003.
- ²⁴S. Xu and M. P. Martin. Assessment of inflow boundary conditions for compressible turbulent boundary layers. *Physics of Fluids*, 16(7):2623–2639, 2004.